1997, 67th Ann. Internat. Mtg., Soc. Expl. Geophys., Expanded Abstracts

Mesaverde and Green River shale anisotropies by wavefront folds and interference patterns

Vigen Ohanian, PGS Tensor; Thomas M. Snyder, Lincoln-Land College; Jose Carcione, OGS*

SUMMARY

Multicomponent seismic acquisition is now considered central to quality geophysical data processing. The additional information provided by multicomponent data offers an opportunity to assess the nature of anisotropy in the subsurface. One of the remarkable effects of anisotropy on acoustic waves is the possibility of the appearance of folds (triplications) in wavefronts. Fold structures in the propagating wavefronts can have striking effects on the observed field records: (a) Folded wavefronts will give rise to folded structures on field records. (b) At trace locations associated with points where folded wavesurfaces intersect, significant wave energy will concentrate. (c) Displays of frequency slices through the field data, will exhibit rings of interference patterns.

In this paper, using data from Mesaverde and Green River shales, we have investigated some of the geophysical implications of the above mentioned effects, attributable to fold phenomenon. Three dimensional displays of group velocities offer vivid demonstrations of folds in wavefronts. Synthetic shot records computed from travel time curves are shown to agree with those obtained from the pseudo spectral solutions of the wave equation. The ability of a single anisotropic wave to interfere with itself is treated analytically, and is illustrated using numerical results from Mesaverde clayshale.

INTRODUCTION

The physical properties of elastic wave propagation in anisotropic media are well known (Auld 1973). In particular, the transversely isotropic (TI) system has been analyzed extensively in the geophysical literature. Exact solutions for phase velocities and polarization vectors for the TI system are known (Daley and Hron, 1977). For weak anisotropy, the first order approximations of these exact solutions, which are substantially simpler and more insightful than their exact counterparts, were obtained by Thomsen (1986). Perturbation theory provides an alternative way to obtain the same approximations without the need of the exact solutions (Ohanian 1996).

In an anisotropic medium, just as in the isotropic case, there are three distinct modes of acoustic wave propagation which are characterized by the fact that their polarization vectors are mutually orthogonal. However, due to anisotropy, the directions of these polarization vectors are no longer exactly parallel or perpendicular to the wavevector $\vec{k}$. Thus, when dealing with anisotropic systems, one speaks of quasi-longitudinal and quasi-transverse waves. Furthermore, in an anisotropic medium the group velocity, which governs the rate of flow of vibrational energy in a plane wave, is generally not along the direction of its wavevector.

For the TI system, because of the rotational symmetry about the vertical axis, the horizontally polarized shear wave decouples from the other two modes. Thus, the three modes of wave propagation in the TI system are properly referred to as qP, qSV, and SH waves.

One of the remarkable consequences of anisotropy in acoustic media is the possibility of the appearance of folds (triplications) in the wavefronts (Maris, 1983). Our numerical investigations with synthetic data suggests that of the two possible transverse modes in a TI system, the qSV mode is the most susceptible to exhibiting folds. We have looked into the wavefront characteristics of all the TI rock data provided by Thomsen (1986). The qSV wavefronts for nearly one fourth of the data were folded. The fold characteristics seen in the qSV wavefronts of Mesaverde clayshale (5501), and Green River shale are quite representative of this group. Thus, we have used data from these two rock types to investigate some of the geophysical implications of folded wavefronts.

Surprisingly, despite the very striking effects that folded wavefronts can give rise to in the observed field records, little attention has been given to this phenomenon in the geophysical literature. Helbig (1966), as well as, Tsvankin and Thomsen (1994) have discussed aspects of folded wavefronts as they relate to the strength of anisotropy and nonhyperbolic moveout. However, as far as we are aware, there are no published accounts of the geophysically observable fold related phenomenon which we describe here.

In this paper, using the anisotropy parameters for Mesaverde and Green River shales (Thomsen, 1986) and working with the exact phase velocity expressions for the TI system, we have numerically computed group velocities and travel-time curves for simple models. Three dimensional displays of the group velocities, which represent the observable wavefronts in the two rock types, offer physical insights into the structure of folds in TI systems. Travel time curves representing field records are in good agreement with synthetics obtained from the pseudo spectral solution of the wave equation. Aspects of the processing implications of fold structures, as they appear on synthetic field records, are also discussed. The remarkable ability of a single acoustic wave to interfere with itself constructively and destructively is treated analytically and is illustrated using numerical results from Mesaverde clayshale.

WAVEFRONTS

Exact solutions for phase velocities for the TI system have been extensively discussed in the geophysical literature (Levin 1978). Assuming $v(\theta)$ is the exact phase velocity for any of the modes in the TI system, then, as it is well known (Byun 1984), the group velocity may be computed by:

$$\vec{V}(\theta) = \frac{dv(\theta)}{d\theta}\hat{e}^{(1)} + v(\theta)\hat{e}^{(3)} \tag{1}$$

where θ, is the angle of the wavevector from the vertical axis of symmetry of the TI system. The mutually orthogonal unit vectors $\hat{e}^{(1)}$, $\hat{e}^{(2)}$ and $\hat{e}^{(3)}$ are such that $\hat{e}^{(3)}$ lies in the direction of the wavevector $\vec{k} = k\hat{e}^{(3)}$. Thus, $\hat{e}^{(1)}$ and $\hat{e}^{(3)}$ define the plane of polarization for qP and qSV modes, and $\hat{e}^{(2)}$ is exactly parallel to the polarization of the SH mode. From Eq. (1) it is evident that the group velocity vector is deviated from the direction of the wavevector. The direction of group velocity from the vertical axis is obtained by:

$$\phi = \theta + \tan^{-1}\left(\frac{dv/d\theta}{v}\right). \tag{2}$$

Using equations (1) and (2), and equipped with the exact expressions for phase velocities for a TI system we have generated three dimensional displays (Fig. 1) of group velocity surfaces for Mesaverde clayshale (5501), and Green River shale (Thomsen 1986).

Group-velocity surfaces displayed in Fig. (1), represent the observable acoustic wavefronts when a point source is embedded inside the body of each rock. Evidently, these wavefronts reflect the basic anisotropies in the two rock types. Because of the symmetry about the vertical axis in the TI system, all of the wavefronts exhibit a cylindrical symmetry. Wavefronts for the qP and the SH modes are seen to be highly non-spherical but do not develop folds. The qSV modes, on the other hand, are folded for both rocks. The folds for the Mesaverde qSV wavefront appear as two cone like structures at the top and bottom, and there is a continuous strip of fold around the middle. Folds for the Green River qSV mode consist of two continuous rings, one at the top and the other at the bottom.

SYNTHETIC SHOT RECORDS

One of the geophysical implications of folds in propagating wavefronts is that, they give rise to folded structures in the observed field records. In this section, we investigate this issue on synthetics, using data from Mesaverde clayshale (5501) and Green River shale. Ray theoretic as well as wave equation solutions for the synthetic shot records are considered.

Assuming z_0 is the reflector depth, then for a given phase angle θ, the travel time t and the offset x can be computed by:

$$t = \frac{2z_0}{|\vec{V}|\cos\phi} \tag{3}$$

and,

$$x = 2z_0 \tan\phi \tag{4}$$

where, $\vec{V}(\theta)$ and $\phi(\theta)$ were defined by Eqs. (1), and (2). Thus, by treating θ as an independent parameter, travel time curves representing filed records may be generated by plotting $t(\theta)$ versus $x(\theta)$.

The synthetic shot records for Mesaverde and Green River shales obtained by ray theoretic and wave equation solutions

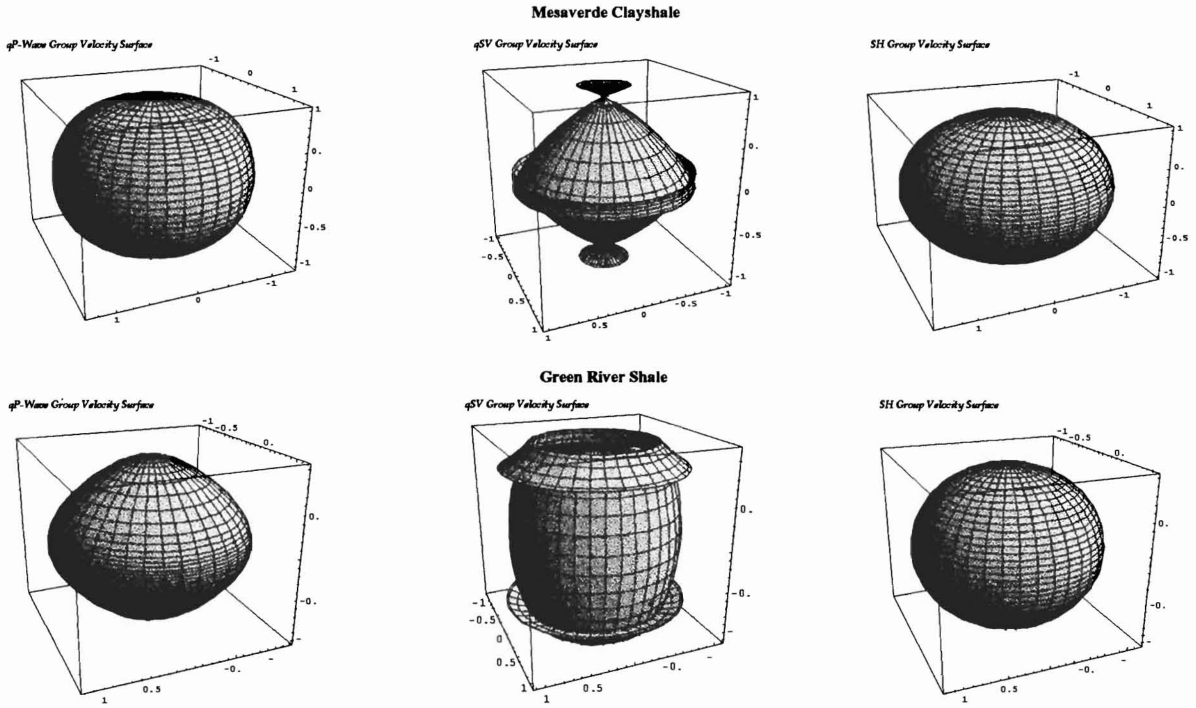

Figure 1: Wavefronts for Mesaverde and Green River shales

are shown in Figs. (2) and (3). For these figures $z_0 = 2500.0$ *feet* was used. The ray theoretic solutions for synthetics, shown in Fig. (2), exhibit all three modes of wave propagation *q*P, *q*SV, and SH. The synthetic shot field records shown in Fig. (3), modeled only the *q*P, *q*SV modes, and were obtained by the pseudo spectral solution of the wave equation. The travel time curves, and shapes of the structures seen on the ray theoretic solutions for the synthetic data, are in agreement with those appearing on the wave equation solutions.

A striking feature revealed on these synthetics, is the appearance of fold structures associated with the *q*SV modes, which are attributable to the folds on the wavefronts. Thus, for certain offsets associated with this single wave mode, a train of multiple events are observed on each trace. These synthetics show that the multiple events, belonging to the *q*SV modes, occur at the near offsets for Mesaverde clay shale, whereas they occur at the far offsets of Green river shale.

Referring to the *q*SV fold structure of the Mesaverde synthetic data, we note that the wave does not arrive first at the zero offset. Rather, since the group velocities of this mode increase in directions slightly away from the vertical, the arrival times decrease with offset up to the cusp of the fold. Thus, giving rise to a concave travel time curve, which defines the top of the fold. Referring to the trailing events which define the bottom of the fold, we note that they arrive simultaneously on the zero offset trace. For wavelengths smaller than the size of the fold, this simultaneously arriving energy on the zero offset trace will cause a significant concentration of wave energy. Similar observation can be made regarding the Green River synthetics.

The appearance of fold structures on field records, raise some interesting processing questions. For the Mesaverde clayshale model with a horizontal reflector, exemplified in Fig. (2), a DMO operator would have to migrate single events from far offset locations, or arrays of triple events from near offset locations, to a zero offset trace which contains two events. In view of the wavefronts shown in Fig. (1), the migration impulse response for the qSV mode will be folded. Maximum energy ray tracing techniques used in PSDM will only account for one of the events on the folded wavefront.

INTERFERENCE PATTERNS

Another remarkable consequence of folded wavefronts is the development of interference fringes observable on frequency slices through field data. In this section this unusual ability of a single acoustic wave to interfere with itself is treated analytically and is illustrated numerically.

A portion of a field record that contains a fold is depicted in Fig. 4. A reflected ray is also shown along the broken line that emerges at offset *x*, and intersects the fold at two points a, and b. Emerging from a depth of z_0, the reflected ray angle ϕ_x from the vertical is given by Eq. (4). The two points a, and b indicated on the figure, correspond to the same offset *x*, but to different $\bar{k}$ directions, θ_a, and θ_b. In what follows, the

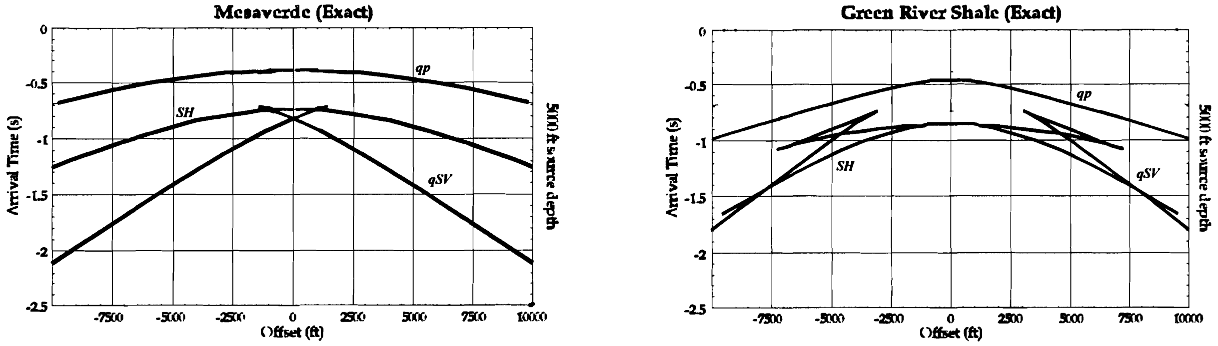

Figure 2: Synthetic shot records by ray theoretic solution

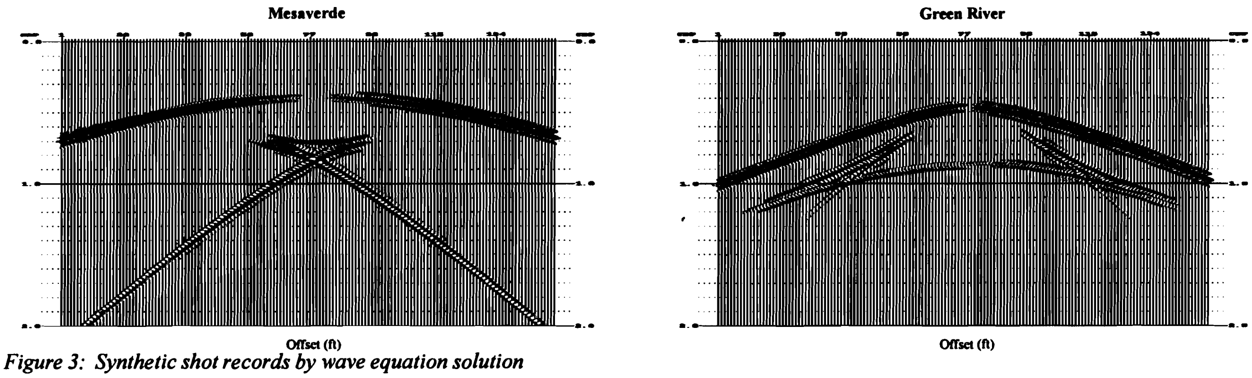

Figure 3: Synthetic shot records by wave equation solution

superposition of two plane waves of same frequency ω, but different wavevectors $\bar{k}_a$, $\bar{k}_b$ will be analyzed.

The two phase angles θ_a, and θ_b can be computed numerically by finding the roots of the $\phi(\theta)-\phi_x=0$, where $\phi(\theta)$ is given by Eq. (2). The wave vector associated with θ_a is $|\bar{k}_a|=\omega/v(\theta_a)$, where $v(\theta_a)$ is the phase velocity. Thus,

$$\bar{k}_a = k_a \sin(\theta_a)\hat{x} - k_a \cos(\theta_a)\hat{z}. \tag{5}$$

Similarly, from θ_b the wavevector $\bar{k}_b$ can be computed. Now, the two plane waves which interfere at offset x are,

$$u_a = u_{0,a}\sin(\bar{k}_a.\bar{r}-\omega t), \tag{6}$$

and

$$u_b = u_{0,b}\sin(\bar{k}_b.\bar{r}-\omega t), \tag{7}$$

where $\bar{r}=x\hat{x}+z\hat{z}$. The resultant of the superposition of the two waves is given by u_a+u_b. Here we also assume the amplitudes of the two interfering waves to be equal, i.e., $u_{0,a}=u_{0,b}\equiv u_0$. Then, the wave intensity which is proportional to the square of the amplitude of the resultant is given by:

$$I=\frac{I_0}{r^2}\cos^2[\frac{1}{2}(\bar{k}_a-\bar{k}_b).\bar{r}]. \tag{8}$$

where $I_0=4u_0^2$, and $r=\sqrt{x^2+z^2}$. The inverse squared r term in the above, accounts for the fall off of intensity with distance.

Using expression (8), and invoking the inherent cylindrical symmetry of the TI system, we have generated displays of the wave intensities for Mesaverde clayshale (Fig 5). The interference fringes seen on the 20 Hz and 40 Hz frequency slices demonstrate the interference process. Fringe spacings exhibit the intimate relationship between fold size and the wavelength.

CONCLUSIONS

In this paper some of the geophysical implications of folds in anisotropic wavefronts are investigated. To this end, data from Mesaverde clayshale (5501), and Green River shale are used. Three dimensional displays of group velocity surfaces offer graphical insights into the observable folds in elastic wavefronts. The qSV mode is the most susceptible to developing folds.

Travel time curves and fold structures seen on the ray theoretic solution of synthetic shot records agree with those obtained from the solution of wave equation. Folds on the Mesaverde synthetics occur at near offsets, whereas, those for the Green River occur at far offsets. The possibility of focusing significant wave energies, attributable to fold structures, are briefly discussed. Some processing issues relating to fold phenomenon are also pointed out.

The remarkable ability of a single anisotropic wave to interfere with itself is treated analytically, and is illustrated using numerical results from Mesaverde clayshale. Interference fringes seen on frequency slices, demonstrate the physical relationship between wave frequency and the fold size.

ACKNOWLEDGMENTS

We thank members of the Technology Department at PGS Tensor, particularly Dr. Matt Brzostowski, for many helpful discussions and suggestions. We also thank Dr.Turgut Ozdenvar, also of PGS Tensor (Technology), for generating snap shots from pseudo-spectral solutions of anisotropic wavefields.

REFERENCES

Auld, B.A., 1973, Acoustic waves and fields in solids: Wiley.

Byun, B. S., 1984, Seismic parameters for transversely isotropic media: Geophysics **49**, 1908-1914.

Daley P. F., and Hron, F., 1977 Reflection and transmission coefficients TI media: Bull., Seis. Soc. Am. **67**, 661-675.

Helbig, K., 1966, A graphical method for construction of rays and travel times in spherically layered media, part 2: anisotropic case, theoretical considerations, Bull. Seis. Soc. Am., **56**, 527-559.

Levin, F. K., 1979, Seismic velocities in transversely isotropic media: Geophysics, **44**, 918-936.

Maris, H.J., 1983, Phys. Rev., Effect of finite phonon wavelength on phonon focusing, **B28**, 7033-7037.

Ohanian, V. 1996, Weak transverse isotropy by perturbation theory: 66th Ann. Internat. Mtg., Soc. Expl. Geophys., Expanded Abstracts 1838-1841

Thomsen, L. A. 1986, Weak elastic anisotropy: Geophysics, **51**, 1954-1966.

Tsvankin, I., Thomsen L. A. 1994, Nonhyperbolic reflection moveout in anisotropic media: Geophys., **59**, 1290-1304.

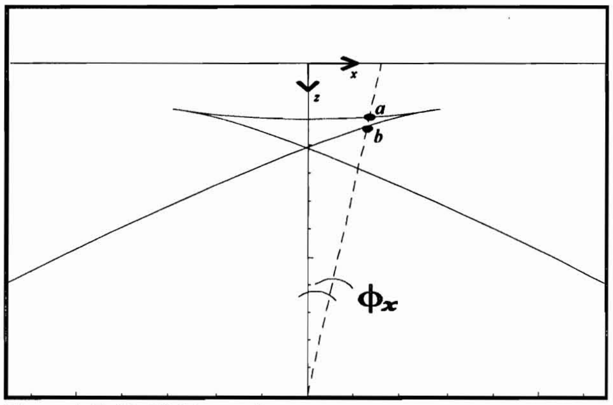

Figure 4: Folded field record

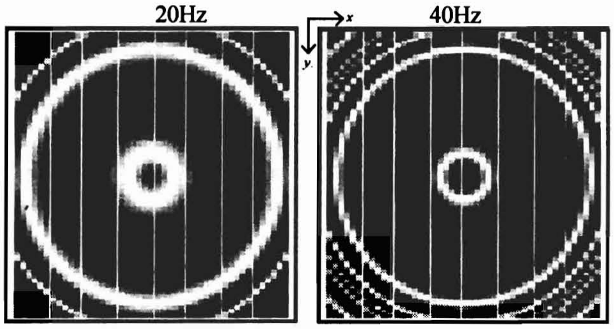

Figure 5: Interference patterns